Dear Author,

Please use this PDF proof to check the layout of your article. If you would like any changes to be made to the layout, you can leave instructions in the online proofing interface.

Making your changes directly in the online proofing interface is the quickest, easiest way to correct and submit your proof. Please note that changes made to the article in the online proofing interface will be added to the article before publication, but are not reflected in this PDF proof.

If you would prefer to submit your corrections by annotating the PDF proof, please download and submit an annotatable PDF proof by following this link:

https://rscweb.proofcentral.com/en/offline.html?token=7bde29c7d89baca7b3b01f36eb590095

Catalysis Science & Technology d0cy00289e

We have presented the graphical abstract image and text for your article below. This briefly summarises your work, and will be presented with your article online.

Q2

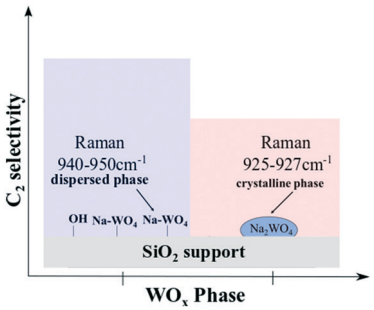

Synthesis and molecular structure of model silica-supported tungsten oxide catalysts for oxidative coupling of methane (OCM)

Daniyal Kiani, Sagar Sourav, Israel E. Wachs* and Jonas Baltrusaitis*

The molecular and electronic structures and chemical properties of the active sites on the surface of supported Na_2WO_4/SiO_2 catalysts used for oxidative coupling of methane (OCM) are poorly understood.

Please check this proof carefully. Our staff will not read it in detail after you have returned it.

Please send your corrections either as a copy of the proof PDF with electronic notes attached or as a list of corrections. **Do not edit the text within the PDF or send a revised manuscript** as we will not be able to apply your corrections. Corrections at this stage should be minor and not involve extensive changes.

Proof corrections must be returned as a single set of corrections, approved by all co-authors. No further corrections can be made after you have submitted your proof corrections as we will publish your article online as soon as possible after they are received.

Please ensure that:

- The spelling and format of all author names and affiliations are checked carefully. You can check how we have identified the authors' first and last names in the researcher information table on the next page. **Names will be indexed and cited as shown on the proof, so these must be correct.**
- Any funding bodies have been acknowledged appropriately and included both in the paper and in the funder information table on the next page.
- All of the editor's queries are answered.
- Any necessary attachments, such as updated images or ESI files, are provided.

Translation errors can occur during conversion to typesetting systems so you need to read the whole proof. In particular please check tables, equations, numerical data, figures and graphics, and references carefully.

Please return your **final** corrections, where possible within **48 hours** of receipt following the instructions in the proof notification email. If you require more time, please notify us by email to catalysis@rsc.org.

Funding information

Providing accurate funding information will enable us to help you comply with your funders' reporting mandates. Clear acknowledgement of funder support is an important consideration in funding evaluation and can increase your chances of securing funding in the future.

We work closely with Crossref to make your research discoverable through the Funding Data search tool (http://search.crossref.org/funding). Funding Data provides a reliable way to track the impact of the work that funders support. Accurate funder information will also help us (i) identify articles that are mandated to be deposited in **PubMed Central (PMC)** and deposit these on your behalf, and (ii) identify articles funded as part of the **CHORUS** initiative and display the Accepted Manuscript on our web site after an embargo period of 12 months.

Further information can be found on our webpage (http://rsc.li/funding-info).

What we do with funding information

We have combined the information you gave us on submission with the information in your acknowledgements. This will help ensure the funding information is as complete as possible and matches funders listed in the Crossref Funder Registry.

If a funding organisation you included in your acknowledgements or on submission of your article is not currently listed in the registry it will not appear in the table on this page. We can only deposit data if funders are already listed in the Crossref Funder Registry, but we will pass all funding information on to Crossref so that additional funders can be included in future.

Please check your funding information

The table below contains the information we will share with Crossref so that your article can be found *via* the Funding Data search tool. **Please check that the funder names and grant numbers in the table are correct and indicate if any changes are necessary to the Acknowledgements text.**

Funder name	Funder's main country of origin	Funder ID (for RSC use only)	Award/grant number
National Science Foundation	United States	100000001	CBET 1706581

Researcher information

Please check that the researcher information in the table below is correct, including the spelling and formatting of all author names, and that the authors' first, middle and last names have been correctly identified. **Names will be indexed and cited as shown on the proof, so these must be correct.**

If any authors have ORCID or ResearcherID details that are not listed below, please provide these with your proof corrections. Please ensure that the ORCID and ResearcherID details listed below have been assigned to the correct author. Authors should have their own unique ORCID iD and should not use another researcher's, as errors will delay publication.

Please also update your account on our online manuscript submission system to add your ORCID details, which will then be automatically included in all future submissions. See here for step-by-step instructions and more information on author identifiers.

First (given) and middle name(s)	Last (family) name(s)	ResearcherID	ORCID
Daniyal	Kiani		0000-0002-9748-3007
Sagar	Sourav		0000-0001-5892-1329
Israel E.	Wachs		
Jonas	Baltrusaitis		0000-0001-5634-955X

Queries for the attention of the authors

Journal: **Catalysis Science & Technology**

Paper: **d0cy00289e**

Title: **Synthesis and molecular structure of model silica-supported tungsten oxide catalysts for oxidative coupling of methane (OCM)**

For your information: You can cite this article before you receive notification of the page numbers by using the following format: (authors), Catal. Sci. Technol., (year), DOI: 10.1039/d0cy00289e.

Editor's queries are marked on your proof like this Q1, Q2, etc. and for your convenience line numbers are indicated like this 5, 10, 15, ...

Please ensure that all queries are answered when returning your proof corrections so that publication of your article is not delayed.

Query Reference	Query	Remarks
Q1	Have all of the author names been spelled and formatted correctly? Names will be indexed and cited as shown on the proof, so these must be correct. No late corrections can be made.	
Q2	Is the inserted Graphical Abstract text suitable? If you provide replacement text, please ensure that it is no longer than 250 characters (including spaces).	
Q3	The sentence beginning "The catalysts prepared…" has been altered for clarity. Please check that the meaning is correct.	
Q4	The meaning of the term "$MnMn_6SiO_2$" in the sentence beginning "To date, almost…" is not clear, please provide alternative text.	
Q5	The sentence beginning "The catalyst samples…" has been altered for clarity. Please check that the meaning is correct.	
Q6	The sentence beginning "The temperature was…" has been altered for clarity. Please check that the meaning is correct.	
Q7	The caption to Fig. 4 has been altered for clarity. Please check that the meaning is correct.	
Q8	"Temperature" appears to be spelled incorrectly as "Temperarture" in Fig. 5b. Please could you supply a corrected version (preferably as a TIF file at 600 dots per inch) with your proof corrections.	
Q9	"products" appear to be spelled incorrectly as "poducts" in Fig. 6. Please could you supply a corrected version (preferably as a TIF file at 600 dots per inch) with your proof corrections.	
Q10	The sentence beginning "Previously, a report…" has been altered for clarity. Please check that the meaning is correct.	
Q11	Have all of the funders of your work been fully and accurately acknowledged?	
Q12	Ref. 16: Please provide the page (or article) number(s).	

Query Reference	Query	Remarks
Q13	Ref. 47: Please give the name of this journal in full, including any other names by which this journal may be known (e.g. Chin. J. Struct. Chem. is also known as Jiegou Huaxue), so that its CASSI abbreviation can be checked for indexing purposes.	
Q14	Please indicate where ref. 49 should be cited in the text.	

Catalysis Science & Technology

ROYAL SOCIETY OF CHEMISTRY

PAPER

Synthesis and molecular structure of model silica-supported tungsten oxide catalysts for oxidative coupling of methane (OCM)†

Cite this: DOI: 10.1039/d0cy00289e

Daniyal Kiani, ‡ Sagar Sourav, Israel E. Wachs* and Jonas Baltrusaitis *

Received 13th February 2020,
Accepted 9th April 2020

DOI: 10.1039/d0cy00289e

rsc.li/catalysis

The molecular and electronic structures and chemical properties of the active sites on the surface of supported Na_2WO_4/SiO_2 catalysts used for oxidative coupling of methane (OCM) are poorly understood. Model SiO_2-supported, Na-promoted tungsten oxide catalysts (Na–WO_x/SiO_2) were systematically prepared using various Na- and W-precursors using carefully controlled Na/W molar ratios and examined with *in situ* Raman, UV-vis DR, CO_2-TPD-DRIFT and NH_3-TPD-DRIFT spectroscopy. The traditionally prepared catalysts corresponding to 5% Na_2WO_4 nominal loading, Na/W molar ratio of 2, were synthesized from the aqueous $Na_2WO_4{\cdot}2H_2O$ precursor. After calcination at 800 °C, the initially amorphous SiO_2 support crystallized to the cristobalite phase and the supported sodium tungstate phase consisted of both crystalline Na_2WO_4 nanoparticles (Na/W = 2) and dispersed surface Na–WO_4 sites (Na/W < 2). The catalysts prepared *via* a modified impregnation method were synthesized using individual precursors of NaOH + AMT, such that the Na/W molar ratio remained well below 2, the resulting SiO_2 remained amorphous and the supported sodium–tungstate phase only consisted of dispersed surface Na–WO_4 sites (Na/W < 2). The dispersed surface Na–WO_4 sites were isolated, more geometrically distorted, less basic in nature, and more reducible than the crystalline Na_2WO_4 nanoparticles. The CH_4 + O_2-TPSR results reveal that the isolated, dispersed surface Na–WO_4 sites are significantly more selective towards C_2 products, and initiate C_2H_6 formation at higher temperature than the traditionally-prepared catalysts that contain both crystalline Na_2WO_4 nanoparticles and dispersed surface Na–WO_4 sites. These findings demonstrate that the isolated, dispersed phase Na–WO_4 sites on the SiO_2 support surface are the catalytically selective-active sites for the OCM reaction.

1. Introduction

Catalytic oxidative coupling of methane (OCM) is a single-step process for the conversion of methane (CH_4) into value-added products such as ethylene (C_2H_4).[1] Since the pioneering work of Kellar and Bhasin in 1982,[2] hundreds of catalysts composed of oxides of alkali, alkaline-earth, and transition metals have been tested for OCM. With the new developments in *in situ* and *operando* measurements, interest in understanding and designing an efficient OCM catalyst has experienced a renewal in the past decade.[3–6] Most of the catalysts reported for OCM were deemed unsuitable for large-scale commercialization due to the lack of long-term stability at high operational temperatures above 800 °C and over-oxidation of hydrocarbons to CO_x.[7,8] In this regard, the SiO_2-supported MnO_x–Na_2WO_4/SiO_2 mixed metal oxide catalyst is one of the few catalysts that exhibit high thermal stability and promising C_2 product yields (~28%).[7,8]

The first reports on the SiO_2-supported MnO_x–Na_2WO_4/SiO_2 catalyst for OCM appeared in the early 90s.[9–12] Since then, research efforts have largely remained focused on increasing the C_2 yield by adding promoters, changing support materials, trying various synthesis routes, *etc.*[7,8] To date, almost all studies conducting characterization of this catalyst have found crystalline phases including Na_2WO_4, Mn_2O_3 and α-cristobalite phases of the SiO_2 support along with $Na_2W_2O_7$, $MnWO_4$ and $MnMn_6SiO_2$, depending on the catalyst preparation method and precursors used.[8] Surprisingly, in the absence of convincing supporting surface site analysis evidence, these crystalline phases have been proposed as active phases towards the catalytic OCM reaction.[7,8,13,14] In contrast, an *in situ* XRD study recently showed that crystalline Na_2WO_4 was not present under OCM reaction conditions (>800 °C) since the Na_2WO_4 crystal melts

Department of Chemical and Biomolecular Engineering, Lehigh University, B336 Iacocca Hall, 111 Research Drive, Bethlehem, PA 18015, USA.
E-mail: iew0@lehigh.edu, job314@lehigh.edu

† Electronic supplementary information (ESI) available. See DOI:10.1039/d0cy00289e

‡ DK and SS contributed equally to this work.

at ~698 °C.[15,16] Additionally, the intensity of the XRD peaks for the crystalline Mn_2O_3 and α-cristobalite phases was found to significantly decrease during OCM, while the intensity of the peaks from the Mn_3O_4 and β-cristobalite phases increased due to phase transformations occurring at OCM relevant temperatures.[8,15,16] These *in situ* XRD results have highlighted that the crystalline phases of Na_2WO_4, Mn_2O_3 and α-cristobalite are not present under OCM reaction conditions and cannot be responsible for the OCM activity, in contrast to previous reports.[8] Unfortunately, information on the stable and active surface structures present on the MnO_x–Na_2WO_4/SiO_2 catalyst at elevated temperatures is largely missing from the literature. Further, prior investigations analyzed the catalysts only under ambient conditions – air-exposed, at room temperature.

Although XRD can readily detect crystalline phases with long-range order, it cannot detect phases lacking long-range order (*e.g.*, amorphous 2D/3D phases and crystalline nanoparticles smaller than 3 nm). In contrast, Raman spectroscopy is better suited to systematically study and understand the molecular structure and identity of phases present on the catalyst support, because it can readily detect and discriminate between amorphous 2D and crystalline 3D phases as well as crystalline nanoparticles lacking long-range order (<3 nm).[17] The few earlier studies that provide Raman spectroscopic characterization of supported MnO_x–Na_2WO_4/SiO_2 catalysts[10,11,18,19] collected information under ambient conditions where the catalyst surface is hydrated by ambient water molecules and differs significantly from the catalyst surface under reaction conditions at elevated temperatures. These reports also contain incorrect and/or unclear Raman band assignments. For example (a) a Raman band at ~950 cm^{-1} was observed, but not assigned,[11] and (b) the distorted tetrahedral WO_4 sites from crystalline Na_2WO_4 and $Na_2W_2O_7$ bulk phases were incorrectly assigned to WO_4 sites anchored to the SiO_2 surface.[10,19] Surface molecular structures of metal oxides will structurally differ from bulk crystalline phases and will be the ones responsible for the structure/reactivity during OCM.[20–23] Recent studies using *in situ* Raman spectroscopy have elucidated the structure of different molecular geometries possible for a SiO_2-supported 2D-dispersed tungsten oxide (WO_x) phase under dehydrated conditions and at elevated temperatures.[17,24–27] Specifically, the dispersed WO_x sites on the SiO_2 support exhibit Raman bands at ~1015 and ~985 cm^{-1} from mono-oxo O═W(O–Si)$_4$ and di-oxo (O═)$_2$W(O–Si)$_2$ sites, respectively.[27] When the maximum dispersion limit of surface WO_x sites on SiO_2 is exceeded, the excess tungsten oxide forms 3D crystalline NPs.[28] Likewise, in the presence of Na, as in the OCM catalyst under discussion, Na-coordinated WO_x sites in the dispersed phase (never reported before) and crystalline Na_2WO_4 (Raman: 925–927, 810, 303 cm^{-1})[26,29] can co-exist. A schematic summary of the crystalline phases and molecular surface structures of the SiO_2-supported WO_x systems is shown in Fig. 1, namely, (a) isolated surface di-oxo sites ([O═]$_2WO_2$) – WO_4, (b) oligomeric surface mono-oxo sites, WO_x ($x \geq 2$) and (c) crystalline WO_3 nanoparticles (NPs) – WO_6.[17,27]

The ability to synthesize and spectroscopically characterize well-defined supported tungsten oxide catalytic sites is essential for establishing conclusive structure–function relationships for OCM.[17,27] This study aims to systematically study the structure of Na–WO_x sites supported on SiO_2. Specifically, the goal is to identify phases, elucidate molecular level structural details, and shed light on fundamental properties of potentially OCM-relevant catalytic sites by tuning the synthesis protocol and adjusting the Na/W molar ratio in a bi-metal oxide configuration containing Na–WO_x sites. Herein, we report on the molecular and electronic structures of the WO_x-based OCM catalytic sites, their domain sizes, their surface properties and their OCM performance. We highlight the effect of using different metal oxide precursors and tuning the Na/W molar ratio of active metal oxides on the final catalyst structure and properties. The catalysts were characterized using *in situ* Raman spectroscopy and *in situ* UV-vis diffuse reflectance spectroscopy and probed using H_2-TPR (temperature-programmed reduction), CH_4 + O_2-TPSR (temperature-programmed surface reaction), and NH_3-TPD-, (temperature-programmed desorption) and CO_2-TPD-DRIFTS (diffuse reflectance infrared Fourier transformed spectroscopy).

2. Experimental

a. Catalyst synthesis

The SiO_2 support (Cabot CAB-O-SIL® EH5 with a surface area of ~332 m^2 g^{-1}) was first treated with water, and then allowed to dry overnight at room temperature before final calcination at 500 °C for 4 hours under flowing air. This treatment increases the density and surface hydroxyls of the SiO_2 support. The dried SiO_2 obtained after calcination was then crushed into fine powder. The resulting pore volume of the SiO_2 powder was determined to be ~0.8 ml g^{-1} and was utilized for all catalyst preparation steps *via* incipient-wetness

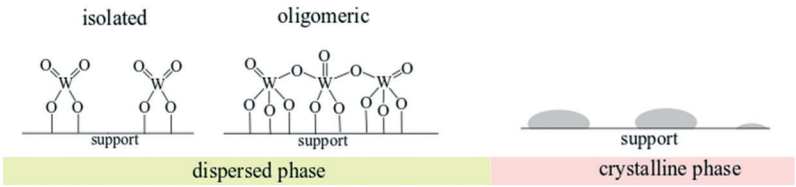

Fig. 1 Schematic representation of possible structural and phase compositions of tungsten oxide-based catalysts on the SiO_2 support.

impregnation (IWI) of the metal oxide aqueous solutions unless mentioned otherwise.

To prepare the supported Na_2WO_4/SiO_2 catalyst with stoichiometric amounts of Na and W oxides, the conventional $Na_2WO_4{\cdot}2H_2O$ (Sigma-Aldrich, 99%) precursor was used. Given that the crystalline Na_2WO_4 phase is not stable under the high-temperature OCM reaction conditions,[15,16] the individual precursors for Na (NaOH (GR ACS, 97%), Na_2CO_3 (Aldrich, 99%) and $NaNO_3$ (Sigma-Aldrich, 99%)) and W (ammonium meta tungstate (AMT, Pfaltz & Bauer, 99.5%) were also utilized in the synthesis of the catalysts. For all preparation steps, the loadings of the Na and W precursors were maintained to correspond to ~5% Na_2WO_4/SiO_2 on a weight basis. After the incipient-wetness impregnation of the metal oxide aqueous solution precursors onto the SiO_2 support, the samples were allowed to initially dry overnight at room temperature followed by additional drying for 2 hours at 120 °C before final calcination at 800 °C for 8 hours under flowing air.

Non-stoichiometric catalysts with the metal oxides fully dispersed on the SiO_2 support were also prepared using a modified IWI method.[30] A NaOH aqueous solution corresponding to the pore-volume equivalent of ~0.8 ml g^{-1} was impregnated onto the SiO_2 support and the sample was initially dried overnight and then at 120 °C in an oven under flowing air for 2 hours, and finally calcined at 700 °C under an air flow for 2 hours. The resultant supported Na/SiO_2 sample, with a pore volume equivalent of ~0.7 ml g^{-1}, was subsequently impregnated with the desired aqueous concentration of W in the form of AMT ($(NH_4)_xW_{12}O_{28}$; Alfa Aesar, #44792). The resultant solid was dried overnight and then at 120 °C for 2 hours in an air flow and finally calcined at 500 °C for 4 hours under flowing air. The final catalysts are denoted as aW/bNa/SiO_2 where a = weight% metal loading of WO_x and b = weight% metal loading of Na. Similar structures and properties were observed for a series of similar catalysts calcined at 800 °C instead of 500 °C. However, the sample prepared *via* 500 °C calcination did not undergo severe sintering typical of higher temperature calcination, enabling easier characterization of the pre-reaction catalytic sites.

b. *In situ* Raman spectroscopy

The *in situ* Raman spectra of the Na coordinated WO_x/SiO_2 supported catalysts were obtained with a Horiba-Jobin Yvon LabRam HR instrument equipped with three laser excitation sources (532, 442, and 325 nm) and a liquid N_2-cooled CCD detector (Horiba-Jobin Yvon CCD-3000 V). The 442 nm laser was chosen for spectral accumulation since it minimizes sample fluorescence from the SiO_2 supported catalysts. The wavenumber calibration was checked using a standard silicon wafer with a Raman vibration at 520.7 cm^{-1}. A confocal microscope with a 50× objective (Olympus BX-30-LWD) was utilized for focusing the laser on the catalysts. Typically, the spectra were collected for 60 s/scan for a total of three scans with a 1000 μm hole with a spectral resolution of ~1 cm^{-1}. Approximately 15–20 mg of each catalyst in the powder form (100–150 μm size range) was loaded into an environmental cell (Harrick, HVC-DR2) with a quartz window with O-ring seals, which was kept cool by circulating cooling water. The *in situ* Raman spectra of the catalysts were collected at 400 °C after dehydration in 10% O_2/Ar (~30 cc min^{-1}) for 60 min.

c. *In situ* UV-vis diffuse reflectance spectroscopy (DRS)

The *in situ* UV-vis spectra of the catalysts were obtained using a Varian Cary 5E UV-vis-NIR spectrophotometer with a Harrick Praying Mantis accessory. Approximately 15–20 mg of each catalyst in the powder form was loaded into an *in situ* Harrick HVCDR2 environmental cell. The UV-vis spectra of the catalyst samples were collected at 400, 120, and 25 °C in the 200–800 nm wavelength range after dehydration (10% O_2/Ar, ~30 cc min^{-1}) for 60 min at 400 °C, using a scan rate of 15 nm min^{-1} and a signal averaging time of 0.6 s. MgO was used as a standard for obtaining the background absorbance which was subtracted from the sample absorbance. The Kubelka–Munk function $F(R_\infty)$ was calculated from the background-subtracted absorbance data of the UV-vis spectrum of each sample. The edge energy (E_g), or bandgap, was determined by finding the intercept of the straight line for the low-energy rise of a plot of $[F(R_\infty)h\nu]^2$ *versus* $h\nu$, where $h\nu$ is the incident photon energy. An example of this calculation can be found in the literature.[31]

d. Temperature programmed techniques

H_2-TPR. The H_2-TPR experiments were carried out using an AMI-200 (Altamira Instruments) with an integrated TCD to record the consumption of H_2 in the exiting gases. Approximately 30 mg of each catalyst sample was loaded (sandwiched between quartz wool beds) into a U-tube sample holder. The catalyst samples were first dehydrated under 10% O_2/Ar (~30 cc min^{-1}) at 400 °C for 60 min, and then cooled down to 100 °C. The H_2-TPR experiments were then performed by ramping the temperature under 10% H_2/Ar (30 cc min^{-1}) at a rate of 10 °C min^{-1} from 100 to 1000 °C.

CH_4 + O_2-TPSR. The CH_4 + O_2-TPSR experiments were also carried out in the AMI-200 system. For these experiments, a Dymaxion Dycor mass spectrometer (DME100MS) was utilized for residual gas analysis. Approximately 30 mg of each catalyst sample was loaded (sandwiched between quartz wool beds) into a quartz U-tube sample holder. The catalyst Q5 samples were first dehydrated under 10% O_2/Ar (~30 cc min^{-1}) at 400 °C for 60 min, and the temperature was then ramped up to 900 °C under an OCM gas mixture (~25 cc min^{-1} of CH_4 and ~40 cc min^{-1} of dry air) and held for 2 hours in order to condition the catalyst under OCM reaction conditions. The catalyst was subsequently cooled to 100 °C under the OCM gas mixture and then purged with Ar (~30 cc min^{-1}) for 30 min. At 100 °C, a very dilute gas mixture of CH_4 + O_2 (CH_4: ~5 cc min^{-1}, 10% O_2/Ar: ~15 cc min^{-1} and Ar: ~80 cc min^{-1}) was introduced and the temperature was

ramped up to 850 °C at 10 °C min^{-1} while analyzing the product gas stream with the online mass spectrometer. The dilution was necessary to prevent damage to the mass spectrometer filament at high O_2 concentrations in the OCM reaction mixture. For the detection of different gases, the following *m*/*z* values were used: CH_4 (16), C_2H_4 (26), CO (28), C_2H_6 (30), O_2 (32), Ar (40) and CO_2 (44). The fragmentation patterns were utilized to find out the mass spectral signal contributions from individual gases for overlapping *m*/*z* values. All reactant and product signals were normalized with the Ar signal, used as an internal standard. Further, the calibration curves were obtained for each reactant (CH_4 and O_2) and product (C_2H_6, C_2H_4, CO and CO_2) for quantification of the mass spectrometer signals of these gases during the experiments. For calibration curve development, at least three different amounts of each gas, diluted in Ar (to make a total flow of ~50 cc min^{-1}), were utilized to enhance accuracy. The conversion (%*X*) of CH_4 and O_2 was determined by the following formula:

$$\%X = \frac{n_0 - n}{n_0} \times 100$$

where n_0 is the number of moles of CH_4 or O_2 in the reactant stream and n is the number of moles of CH_4 or O_2 in the product stream.

The selectivity (%*S*) to each product was determined using the following formula:

$$\%S_i = \frac{n_{C_i}}{\sum n_{C_i}} \times 100$$

where n_{C_i} denotes the number of moles of C atoms present in product i.

Lastly, the yield (%*Y*) of any product i was determined by:

$$\frac{\%X_{CH_4} \times S_i}{100}$$

Surface properties: NH_3- and CO_2-TPD-DRIFTS. The *in situ* DRIFT spectra were collected with a Thermo Nicolet iS50 FT-IR spectrometer equipped with a Harrick Praying Mantis attachment (model DRA-2) for diffuse reflectance spectroscopy. The spectra were taken using an MCT detector with a resolution of ~4 cm^{-1} and an accumulation of 96 scans. Approximately ~20 mg of each catalyst in the powder form was loaded into an environmental cell (HVC-DR2, Harrick Scientific). The collection of the initial background was performed by first optimizing the beam path and IR absorption signal using the height of the full Harrick sample cup and then removing the Harrick cell and placing a reflective mirror in the laser path. A spectrum was collected using the reflective mirror and was used as the background spectrum throughout the experiment. The catalysts were first cleaned and dehydrated at 400 °C under a 10% O_2/N_2 gas mixture at a ~30 ml min^{-1} flow rate, cooled to 120 °C under 10% O_2/N_2 and flushed with UHP5.0 N_2 (Praxair Prospec) at a 30 ml min^{-1} flow rate for ~15 min. The catalysts were then subjected to gas adsorption at 120 °C (1% NH_3 in N_2 or 10% CO_2 in N_2 or UHP5.0 N_2 at a 30 ml min^{-1} flow rate through a methanol containing bubbler) for ~30 min followed by flushing with UHP5.0 N_2 at a 30 ml min^{-1} flow rate for another 30 min to remove residual physisorbed molecules. The temperature was subsequently ramped from 120 to 400 Q6 °C at 10 °C min^{-1}, while a spectrum was collected every minute (accumulation of 96 scans) with a spectral resolution of ~4 cm^{-1}. The spectra of the dehydrated catalysts were subtracted from the spectra of the catalysts containing adsorbed gases at the same temperature.

3. Results

a. *In situ* Raman spectroscopy of model supported Na–WO_x/SiO_2 catalysts

The *in situ* dehydrated Raman spectra of the model catalysts corresponding to 5% Na_2WO_4/SiO_2 nominal composition are presented in Fig. 2. As shown in Fig. 2a, for all the catalysts with a Na/W molar ratio of 2, which mimic the stoichiometry of the Na_2WO_4 crystals and irrespective of the precursor choice, the SiO_2 support is present in the β-cristobalite phase with corresponding bands labeled '#'. In the presence of Na, the starting amorphous SiO_2 converts to crystalline cristobalite during the calcination step at ~800 °C. The exclusive presence of the β-cristobalite phase of SiO_2 in the *in situ* Raman is due to the α-cristobalite transformation into β-cristobalite above 250 °C, as shown in Fig. S1.† The Raman spectra of the supported 5% Na_2WO_4/SiO_2 catalysts prepared using $Na_2WO_4{\cdot}2H_2O$, NaOH+AMT and Na_2CO_3 + AMT exhibit Raman bands at 925, 810 and 303 cm^{-1} that are characteristic of crystalline Na_2WO_4.[26] These catalysts also exhibit a small Raman band at 943 cm^{-1}, appearing as a shoulder to the 925 cm^{-1} band, which does not belong to crystalline Na_2WO_4. The deconvolution of the bands present between 900 and 960 cm^{-1} is shown in Fig. S2.† The Raman spectrum of the supported 5% Na_2WO_4/SiO_2 catalyst prepared using $NaNO_3$ + AMT only exhibits a weak and broad Raman band at 932 cm^{-1} and no sharp bands due to the crystalline Na_2WO_4. Such spectral features suggest the presence of a poorly-ordered phase composed of Na- and W-oxides. The origin of the broad Raman band in the 930–950 cm^{-1} range shown in Fig. 2a is not immediately clear. It can be hypothesized that this band originates due to the Na-coordinated WO_x amorphous sites (Na–WO_x) present on the SiO_2 surface.

Model catalysts with Na/W molar ratios from 0.0 to 1.6 were synthesized and characterized as shown in Fig. 2b. Besides the catalyst with a Na/W molar ratio of 1.6, none of the catalysts exhibit sharp Raman bands at 925, 810 and 303 cm^{-1} corresponding to crystalline Na_2WO_4 indicating that only a dispersed Na–WO_x phase is present on the SiO_2 support. Moreover, Raman bands corresponding to the crystalline cristobalite phase of the SiO_2 support were not observed in these samples, indicating that the SiO_2 support is present in its amorphous phase. Specifically, the supported

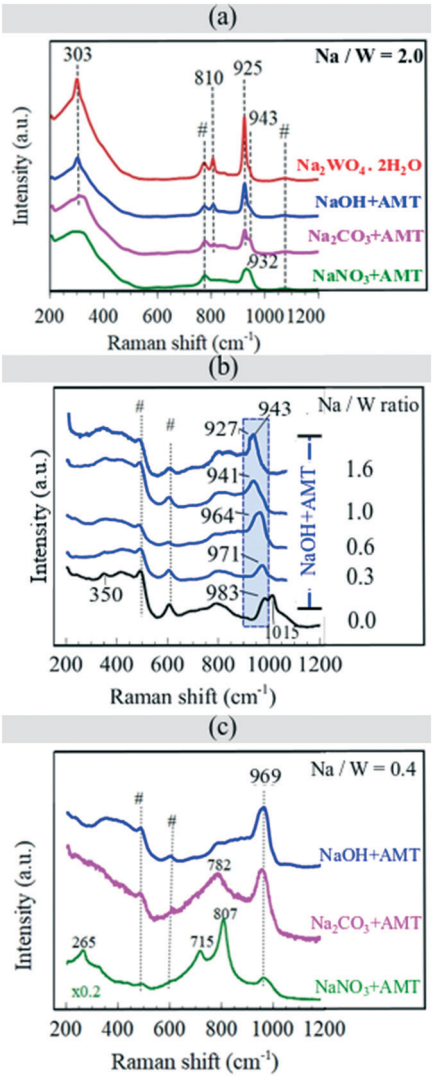

Fig. 2 *In situ* Raman spectra of (a) stoichiometric Na/W = 2 catalysts obtained using different precursors, (b) non-stoichiometric catalysts prepared using different Na/W molar ratios, while keeping precursors (AMT + NaOH) constant (the W═O bond vibration is seen to redshift as the Na/W molar ratio increases from 0.0 to 1.6), (c) non-stoichiometric Na/W = 0.4 catalysts prepared using different precursors. All spectra were collected at 400 °C under dehydrated conditions. '#' indicates Raman bands originating from the SiO_2 support.

5% WO_x/SiO_2 catalyst without any Na-dopant (Na/W = 0) exhibits three characteristic Raman bands at 1015, 983 and 350 cm^{-1} which correspond to the stretching and bending modes of the mono-oxo WO_5 (O═WO_4) and the di-oxo WO_4 ([O═]$_2WO_2$) sites on the SiO_2 surface, respectively.[26,27] Addition of 0.2% Na to the supported 5% WO_x/SiO_2 catalyst to yield Na/W = 0.3 results in a redshift of the W═O Raman vibration from 983 to 971 cm^{-1}. As the Na concentration is further increased to yield larger Na/W molar ratios of 0.6 and 1, the W═O band vibration redshifts further to 964 and finally to 941 cm^{-1}, respectively. At the highest concentration of Na, with the Na/W molar ratio of 1.6, two Raman bands are present at 927 and 943 cm^{-1}. The band at 927 cm^{-1} belongs to the crystalline Na_2WO_4 nanoparticles while the band at 943 cm^{-1} belongs to the surface WO_x sites coordinated to Na (Na–WO_x) as revealed by the spectra of the catalysts with lower Na/W ratios.

Next, the influence of specific Na precursors on the non-stoichiometric catalysts with a low Na content (8% WO_x/0.4% Na/SiO_2; Na/W = ~0.4) is presented in Fig. 2c and reveals the precursor-dependence. The catalyst prepared using the AMT + NaOH precursor yielded only the fully dispersed phase with surface Na–WO_x sites (~969 cm^{-1}) without any crystalline phases like Na_2WO_4 (~925, 810 and 303 cm^{-1}) or WO_3 (715 and 807 cm^{-1}).[26,27] However, when $NaNO_3$ was employed as the Na precursor, mixed phases were observed, with crystalline WO_3 exhibiting sharp, intense bands at 715 and 807 cm^{-1},[26] and dispersed phase Na–WO_x surface sites at 969 cm^{-1}. When the Na_2CO_3 precursor was used, Raman bands were present from surface Na–WO_x sites (~969 cm^{-1}) along with amorphous, poorly-ordered WO_3 NPs (~782 cm^{-1}).[32] The surface Na–WO_x sites are dominant in all the supported 8% WO_x/0.4% Na/SiO_2 catalysts since the Raman cross-sections of the crystalline and poorly-ordered WO_3 NPs are orders of magnitude greater than those of the surface Na–WO_x sites.[33,34]

b. *In situ* UV-vis diffuse reflectance spectroscopy of model supported Na–WO_x/SiO_2 catalysts

The *in situ* UV-vis DR spectra of the supported 5% Na_2WO_4/SiO_2 catalysts prepared using different precursors are shown in Fig. 3 and their corresponding edge energy (E_g) values and ligand-to-metal-charge-transfer (LMCT) band positions are presented in Table S1† while the corresponding Raman spectra of these catalysts are shown in Fig. 2a. The catalysts prepared with the $Na_2WO_4{\cdot}2H_2O$ and NaOH+AMT precursors exhibit a strong LMCT band at ~214 nm and a weaker band

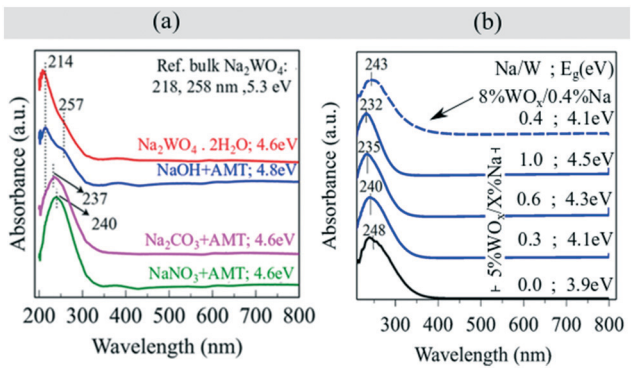

Fig. 3 UV-DRS plots for (a) catalysts prepared using different Na and W precursors, each nominally corresponding to 5% Na_2WO_4/SiO_2 composition and (b) model catalysts prepared with varying Na/W molar ratios, using AMT + NaOH precursors. The dashed plot, labeled 8% WO_x/0.4% Na/SiO_2 (Na/W = 0.4) is significant since such high W loading in a fully dispersed phase has not been reported before. The solid blue plots in (b) use 5% WO_x loadings with corresponding Na loadings to tune Na/W.

at ~257 nm. The strong band at ~214 nm corresponds to the crystalline Na_2WO_4 phase.[26] The band at ~257 nm band is not present in the UV-vis DRS spectrum of crystalline Na_2WO_4 and arises from the dispersed Na–WO_4 surface sites (*vide infra*). The shoulder at ~257 nm for the catalyst synthesized from the NaOH + AMT precursors indicates a slightly higher population of the dispersed Na–WO_4 surface phase than that of the crystalline Na_2WO_4 phase in comparison to the catalyst prepared using the $Na_2WO_4{\cdot}2H_2O$ precursor. For the catalysts prepared from the Na_2CO_3 + AMT and $NaNO_3$ + AMT precursors, a broad and strong UV-vis band is present at ~237–240 nm suggesting comparable signals from crystalline or disordered Na_2WO_4 and dispersed Na–WO_4 surface sites. The absence of UV-vis absorption in the 400–700 nm range indicates that the supported tungsten oxide phases are in their fully oxidized state (W^{6+}).[27] The corresponding UV-vis E_g values for these catalysts are found to be in the narrow range of 4.6–4.8 eV, which is slightly lower than that of the bulk Na_2WO_4 crystalline material (E_g ~ 5.3 eV), and reflect the presence of isolated tetrahedral WO_4 sites (both for crystalline/disordered Na_2WO_4 and dispersed Na–WO_4 sites).[26]

The *in situ* UV-vis DRS spectra of the non-stoichiometric catalysts are presented in Fig. 3b and their corresponding LMCT bands and E_g values are summarized in Table S2.† The UV-vis spectra are dominated by a broad LMCT band that shifts from 247 to 232 nm with increasing Na/W. Moreover, a continuous increase in the E_g value from 3.9 to 4.5 eV was also observed with increasing Na/W ratio. These trends reflect the increase in symmetry of the surface WO_4 sites with increasing Na/W ratio since the corresponding Raman spectra do not indicate the presence of crystalline Na_2WO_4 NPs or bridging W–O–W bonds from oligomeric surface WO_x sites in the 200–300 cm^{-1} range. Increasing the surface WO_x content to 8% and decreasing the surface Na content to 0.4% result in a Na/W ratio of 0.4 (dashed plot) and yield an E_g value of 4.1 eV, which is similar to a previous E_g value for the catalyst with a Na/W ratio of 0.32. Similar to the stoichiometric catalysts (Na/W = 2), the UV-vis DRS spectra of the non-stochiometric catalysts (Na/W < 2) do not contain absorption bands in the 400–700 nm range, indicating the presence of fully oxidized W^{6+} sites.

c. Surface acidity and basicity of model supported Na–WO_4 catalysts

Surface acidity. *In situ* NH_3-TPD-DRIFTS was used to study the surface acidity of the dehydrated catalyst samples. The NH_3-TPD-DRIFT spectra of 5% WO_x/SiO_2 – the only acidic sample as shown in Fig. S3† – are shown in Fig. 4a, from 120 to 400 °C. After NH_3 adsorption at 120 °C, the DRIFT spectrum of the supported WO_x/SiO_2 catalyst with Na/W = 0 exhibited peaks corresponding to NH_3 adsorbed on Lewis acid sites with bands at 1334 and 1615 cm^{-1} and on Brønsted acid sites as surface NH_4^+ ions with a band at 1437 cm^{-1}.[35,36] As the temperature was ramped from 120 to 400 °C, the

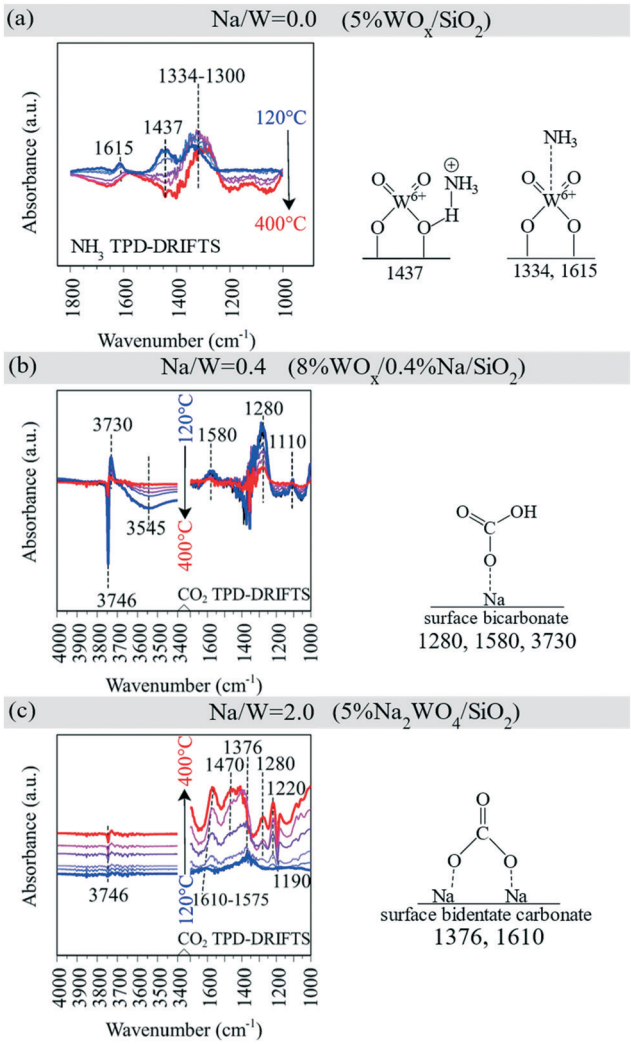

Fig. 4 (a) *In situ* NH_3-TPD-DRIFTS spectra of the 5% WO_x/SiO_2 catalyst (Na/W = 0), prepared using the AMT precursor. *In situ* CO_2-TPD-DRIFTS spectra of (b) the non-stoichiometric 8% WO_x/0.4% Na/SiO_2 catalyst corresponding to Na/W = 0.4, prepared using AMT and NaOH precursors and (c) the stoichiometric 5% Na_2WO_4/SiO_2 catalyst with Na/W = 2, prepared using the $Na_2WO_4{\cdot}2H_2O$ precursor. The corresponding molecular structures of the adsorbed species are shown next to the DRIFTS plot in each case.

surface NH_4^+-species on Brønsted acid sites were not present beyond ~220 °C while the surface NH_3 species on Lewis acid sites were present even at 400 °C, reflecting the stronger acid strength of the surface Lewis acid sites. On the other hand, both of the Na-containing samples, *i.e.* the non-stoichiometric 8% WO_x/0.4% Na/SiO_2 with Na/W = 0.4 and the stoichiometric 5% Na_2WO_4/SiO_2 with Na/W = 2, exhibited no peaks due to NH_3 adsorbed on Lewis or Brønsted acid sites (Fig. S3a†). This indicated that the presence of the small Na concentrations readily removes all surface acidity in the Na–WO_x-based catalysts.

Surface basicity. The DRIFT spectra obtained during CO_2-TPD-DRIFTS from 120 to 400 °C are shown in Fig. 4b and c. Adsorption of CO_2 was negligible on the supported WO_x/SiO_2

catalyst with Na/W = 0 because of the acidic nature of the surface WO_x sites (Fig. S3b†). However, CO_2 readily adsorbed on the Na-containing catalysts due to the interaction between acidic CO_2 and the basic Na^+ cations. For the catalyst with a Na/W molar ratio of 0.4 (Fig. 4b), CO_2 adsorption resulted in a monodentate bicarbonate structure due to the coordination to the isolated surface Na^+ sites, as evidenced by the characteristic 1280 and 3730 cm^{-1} bands due to the O–H bending and stretching, respectively, and the ~1580 cm^{-1} band due to the asymmetric –COO stretching of bicarbonate (–C═O(–OH)).[35,37–40] The negative DRIFTS band at 3746 cm^{-1} corresponds to the consumption of Si–OH hydroxyls on the SiO_2 support upon surface bicarbonate formation. Upon temperature ramping, some surface bicarbonates were still present at 400 °C reflecting the strength of these isolated basic surface sites. Lastly, for the stoichiometric catalyst Na/W molar ratio of 2 (Fig. 4c), CO_2 adsorbed on the surface as bidentate carbonate due to the higher surface density of Na^+ cations allowing for bi-ligation of the CO_2 molecules. IR bands at 1364 and 1610 cm^{-1} correspond to the symmetric and asymmetric stretching of –COO from the surface CO_3 species.[35,37–40] The TPD results reveal the higher basic strength of the surface Na^+ sites as evidenced by the presence of strong IR peaks from surface carbonates even at ~400 °C. In addition, as the temperature was increased, IR peaks at 1570 and 1280 cm^{-1} increased reflecting the formation of surface bicarbonates at higher temperatures.[35,37–40] Note that as seen in Fig. S3b,† bulk Na_2WO_4 also exhibits the formation of bidentate carbonate species upon CO_2 formation, suggesting that the Na densities on bulk Na_2WO_4 and 5% Na_2WO_4/SiO_2 are similar.

d. Temperature-programmed chemical probing studies

H_2-TPR. The H_2-TPR T_p values of the dispersed supported catalysts are sensitive to the Na/W ratio and continuously decrease from ~890–690 °C with increasing Na/W ratio. For the highest Na loading of Na/W = 1.6 shown in Fig. 5a, an additional reduction peak at ~760 °C was observed, which corresponds to the reduction of crystalline Na_2WO_4 (*vide infra*). The H_2-TPR spectra of the stoichiometric (Na/W = 2) 5% Na_2WO_4/SiO_2 catalysts prepared by utilizing different precursors for Na and W oxides are presented in Fig. 5b. The catalyst prepared with the $Na_2WO_4{\cdot}2H_2O$ precursor which contains the highest amount of crystalline Na_2WO_4 phase as shown in the Raman spectrum in Fig. 2 exhibits a strong reduction peak at ~740 °C and a broad reduction peak between 550 and 700 °C (T_p ~ 640 °C) originating from crystalline Na_2WO_4 and dispersed Na–WO_4 sites, respectively. The deconvolution of the two reduction regimes was undertaken and a ratio of the contribution of dispersed Na–WO_4 sites to the crystalline Na_2WO_4 phase towards the total reduction profile is given in Table S3.† These H_2-TPR features are also present for the other catalysts (5% Na_2WO_4/SiO_2 prepared from AMT + NaOH and AMT + Na_2CO_3) with slight shifts in the T_p values. Namely, (i) the T_p value for the Na_2WO_4 NPs shifts from ~740 to ~690 °C as the particle size decreases because of the easier reduction of smaller particles and (ii) the T_p values for the dispersed Na–WO_4 sites are strongly dependent on the quantity of interacting surface Na cations and shift from ~890 to 640 °C. The H_2-TPR spectrum of the catalyst prepared from the AMT + $NaNO_3$ precursors is the most unusual since this sample doesn't exhibit the Raman features of crystalline Na_2WO_4 NPs (see Fig. 2a) and contains two broad reduction bands centered at ~640 and ~820 °C from surface Na–WO_4 species containing variable local Na concentrations, respectively. The lower T_p values for the dispersed phase Na–WO_4 sites with the Na/W concentration much lower than 2 demonstrate that the surface non-stoichiometric Na–WO_4 sites can reduce with H_2 more readily than the crystalline Na_2WO_4 phase, which contains Na/W stoichiometry of 2.

(CH_4 + O_2)-TPSR. The (CH_4 + O_2)-TPSR spectra for the non-stoichiometric catalyst with a Na/W molar ratio of 0.4 and the stoichiometric catalyst with a Na/W ratio of 2 are shown in Fig. 6. The 8% WO_x/0.4% Na/SiO_2 (Na/W = 0.4) catalyst exhibits a light-off temperature for selective product C_2H_6 of ~650–670 °C, while no C_2H_4 evolved over this catalyst. The unselective product, *i.e.* CO, exhibits a light-off

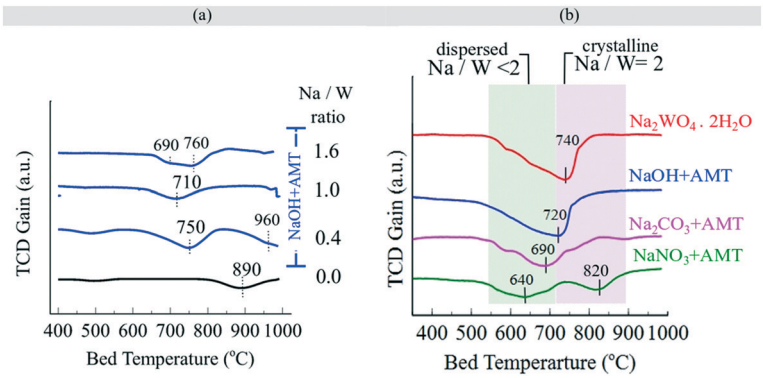

Q8 **Fig. 5** H_2 temperature-programmed reduction (H_2-TPR) for (a) non-stoichiometric, dispersed phase catalysts with Na/W = 0–1.6 and (b) 5% Na_2WO_4/SiO_2 (Na/W = 2) prepared with various precursors.

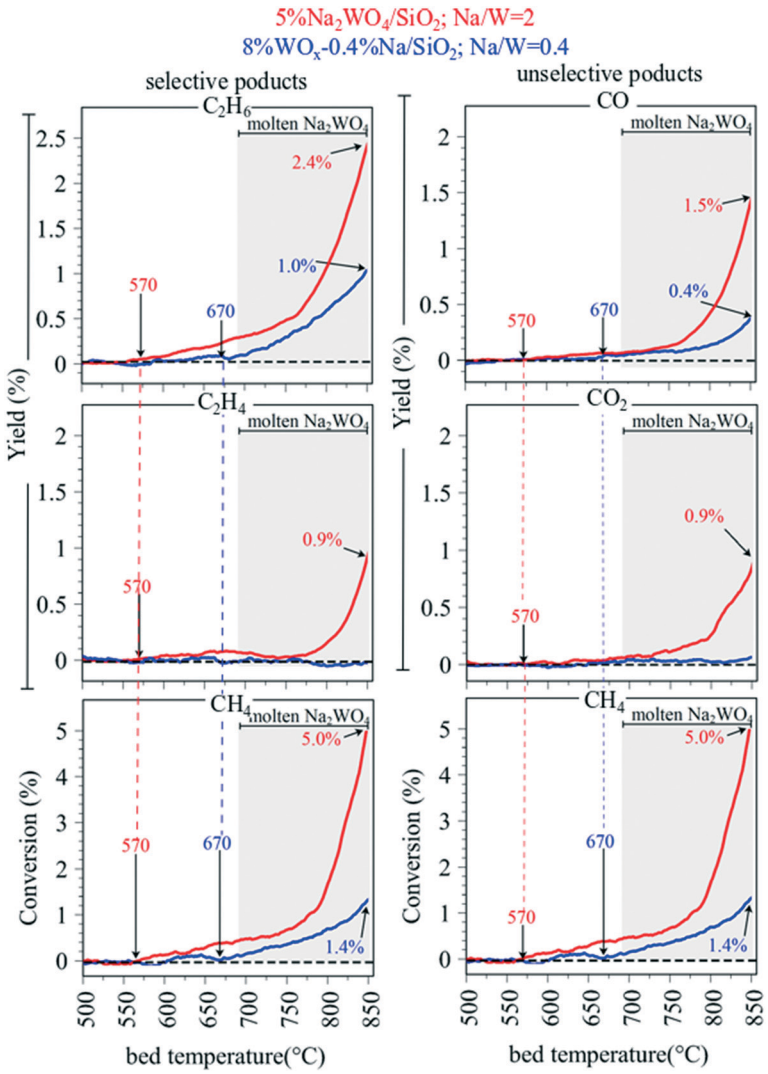

Fig. 6 $CH_4 + O_2$ temperature-programmed surface reaction (TPSR) for 8% WO_x/0.4% Na/SiO_2 (Na/W = 0.4), shown in blue, and 5% Na_2WO_4/SiO_2 (Na/W = 2) prepared from the $Na_2WO_4{\cdot}2H_2O$ precursor, shown in red. A heating rate of 10 °C min^{-1} was used for this TPSR study.

temperature of ~670 °C, while appreciable amounts of CO_2 are not detected from the catalyst. On the other hand, the light off temperatures for selective products on the Na/W = 2 catalyst were 570–590 °C for both C_2H_6 and C_2H_4, although a strong evolution of C_2H_4 was observed above 800 °C. In terms of unselective products, considerable amounts of CO and CO_2 co-evolved with the selective C_2 products at 570–590 °C on this catalyst.

The ($CH_4 + O_2$)-TPSR results herein reveal that:

a) CH_4 conversion starts at ~570–590 °C on the Na/W = 2 catalyst, and at 670–690 °C on the Na/W = 0.4 catalyst, which suggests that higher Na/W creates more reducible sites (as shown in Fig. 5) that are more active towards OCM. (Reducibility ↑, activity ↑)

b) The C_2 ($C_2H_6 + C_2H_4$) yield is 3.3% and the CO_x (CO + CO_2) yield is 2.4% for the Na/W = 2 catalyst, leading to a selectivity of ~58% (selective yield/total yield = ~0.58). On the other hand, for the Na/W = 0.4 catalyst, the C_2 yield is 1%, while the CO_x yield is 0.4%, *i.e.* selectivity of ~71%.

4. Discussion

a. Molecular and electronic structures of model SiO_2-supported tungsten oxide catalysts

Molecular level resolved model OCM catalysts with distinct phases and molecular structures were synthesized and investigated systematically to study their molecular structures and properties. The experimental results in Fig. 2a, S2† and 3a show that the 5% Na_2WO_4/SiO_2 OCM catalysts contain (a) a fully dispersed Na–WO_4 phase consisting of isolated WO_4 units with a Na/W molar ratio less than 2, (b) a crystalline Na_2WO_4 phase with a Na/W ratio of 2 and (c) a SiO_2 support in the β-cristobalite phase. Interestingly, by using different Na and W oxide precursors for preparing the catalysts with the same nominal loading of ~5% Na_2WO_4/SiO_2, it was shown that the ratio between the fully dispersed Na–WO_x (Raman band at ~943 cm^{-1}) and the crystalline Na_2WO_4 (Raman band at 925 cm^{-1}) phases could be controlled and the catalysts prepared using individual Na and W precursors

exhibit higher amounts of the dispersed Na–WO_4 surface sites.

For the Na/W < 2 catalysts which contain only dispersed phase Na–WO_4 surface sites, the SiO_2 support is present in its amorphous phase instead of the crystalline β-cristobalite phase. Their molecular structure, shown in Fig. 2b, is highly distorted pseudo-tetrahedral WO_4 coordinated to Na cations that cause elongation of the W═O bond, as suggested by W═O Raman band red-shifting with an increase in the Na/W ratio. This trend matches previous reports that also showed that when an alkali metal, such as K, is doped into supported WO_x catalysts, the W═O vibration of the surface WO_x sites shifts to lower values by 30–80 cm^{-1} suggesting the strong interactions between the alkali dopant and the oxygen bound to the WO_x sites.[28] Like the Na/W = 2 catalysts, the Na/W < 2 catalysts also exhibit a strong precursor-dependent phase generation behavior where the formation of dispersed Na–WO_4 surface sites is generally greater for preparation with low Na/W ratios (lower than 1.6) and the use of AMT + NaOH as the precursors. On the other hand, as seen in Fig. 2c, crystalline phases formed when Na precursors with lower pH were used ($NaNO_3$ or Na_2CO_3). Finally, the electronic structure information in Fig. 3b corroborates that as the Na/W molar ratio increases, the distortion in the tetrahedral geometry of the WO_4 units decreases, as evidenced by an increase in the E_g values. When the Na/W ratio is high enough that locally it is ~2, crystalline Na_2WO_4 nanoparticles form and the E_g increase approaches that of the bulk, unsupported crystalline Na_2WO_4 at 5.3 eV.

In summary, the molecular structures of the SiO_2-supported tungsten oxide phases are strongly dependent on the synthesis method (specific precursor and Na/W ratio), which allows for controlling the distribution of various possible phases on the SiO_2 support. The characterization results herein clearly reveal that the Na–WO_x/SiO_2 catalyst can contain four distinct structural regimes, namely, crystalline Na_2WO_4 with Na/W = 2, crystalline WO_3 with Na/W = 0, dispersed Na–WO_4 with Na/W < 2, and dispersed WO_4 with Na/W = 0. Except for the crystalline WO_3 phase composed of extensive oligomeric W^{6+} sites, the three other tungsten oxide structures consist of isolated W^{6+} centers.

b. Nature of surface sites in model SiO_2-supported tungsten oxide catalysts

The molecular structures present in the SiO_2-supported tungsten oxide catalysts possess different surface acidity–basicity characteristics. The dispersed WO_4 surface sites and crystalline WO_3 nanoparticles in a catalyst with Na/W = 0 exhibit surface Lewis and Brønsted acidity (see Fig. 4). In the presence of surface Na, the acidic surface WO_4 sites are transformed into basic surface sites as the Na cations coordinate to the WO_x centers forming surface Na–WO_4. The degree of basicity of Na-coordinated surface WO_4 sites strongly depends on the Na/W ratio. At Na/W = 0.4, surface monodentate bicarbonate species formed. On the other hand, at Na/W = 2, both in bulk Na_2WO_4 and in 5% Na_2WO_4/SiO_2, surface bidentate carbonate species formed, suggesting similar surface Na density in both cases.

The redox properties of the molecular structures present in the SiO_2-supported tungsten oxide catalysts were probed with H_2-TPR. The Na-free SiO_2-supported WO_4 sites were quite stable towards the reduction and exhibited a T_p value of ~890 °C. The addition of Na, however, dramatically enhanced the reduction of the surface WO_4 sites, indicated by lowering of the T_p value from ~890 °C (Na/W = 0) to ~710 °C (Na/W = 1). The reduction of the SiO_2-supported crystalline Na_2WO_4 NPs varied over a smaller range from T_p values of 740 to 690 °C with decreasing size of the Na_2WO_4 NPs. In the presence of significant concentrations of Na, the reduction of the surface Na–WO_4 NPs by H_2 becomes more facile.[41–47] The H_2-TPR reduction profiles of supported Na_2WO_4/SiO_2 catalysts have been previously investigated[45–47] and reported a major reduction peak at 720–750 °C that was assigned to the reduction of the crystalline Na_2WO_4 phase.[45,47] This assignment is in agreement with the reduction peak in the 690–740 °C range, for our 5% Na_2W_4/SiO_2 catalysts, associated with the reduction of crystalline Na_2WO_4 NPs. In addition to the significant reduction in the 720–750 °C range, the H_2-TPR profiles in the literature also exhibited a weak, broad reduction peak in the lower temperature range of 625–675 °C, but the authors could not explain the origin of this peak.[28,45,47] The work herein reveals, for the first time, that the lower H_2 reduction peak is due to the presence of dispersed phase Na–WO_4 surface sites in these catalysts that were also present in the catalysts previously reported, but not identified.

c. Catalytic properties of surface sites in model SiO_2-supported tungsten oxide catalysts for OCM

The catalytic performance of the SiO_2 supported Na–WO_x catalysts is investigated by CH_4 + O_2 TPSR experiments. The results (in Fig. 6 along with results presented in Fig. 2–5) suggest that the 5% Na_2WO_4/SiO_2 catalyst with strongly basic sites present as a mixture of crystalline and dispersed phases, with Na/W = 2 and Na/W < 2, respectively, led to co-evolution deep-oxidation products under OCM reaction conditions. However, the 8% WO_x/0.4% Na/SiO_2 catalyst, which only contains mildly basic, dispersed phase Na–WO_4 sites with Na/W = 0.4, suppresses the formation of deep-oxidation products, albeit their lower activity. The distinct chemical properties of the stoichiometric Na/W = 2 *versus* the non-stoichiometric Na/W = 0.4 sites in WO_x-based catalysts towards methane activation during OCM introduce an often-overlooked parameter for tuning the selectivity of the active centers by varying the Na/W ratio in these catalysts. OCM selective catalytic sites originating from the dispersed phase instead of the crystalline phase of the catalyst were acknowledged only indirectly in a recent study which concluded that reducing the overall catalyst loading reduced

the size of the Na_2WO_4 crystallites, leading to an increase in the catalytic activity of the catalyst.[48]

Q10 Previously, a report[45] investigating the effect of using different precursors for Na and W observed that a catalyst made by impregnating the $Na_2WO_4{\cdot}2H_2O$ precursor into synthetic α-cristobalite yielded poorer catalytic activity than the one prepared by impregnating the precursor into amorphous SiO_2, which then transformed into cristobalite *in situ* during calcination. The H_2-TPR results of the same study, for the Na_2WO_4/SiO_2 catalyst prepared using the amorphous SiO_2 support, reported a reduction peak at ~625 °C (on the shoulder of the 750 °C reduction peak from the crystalline Na_2WO_4 phase) corroborating the reduction behavior observed in this work for surface Na–WO_4 sites with Na/W ≪ 2. It can be suggested that as amorphous SiO_2 transforms into the cristobalite phase during calcination, facile Na^+ ions migrate into the SiO_2 bulk leading to a decrease in the surface Na concentration, effectively generating dispersed phase Na–WO_4 surface sites with Na/W < 2, which are significantly more C_2 selective, but less active for OCM.

Other authors investigated the interactions of Na–WO_x oxides in the catalyst and concluded that the WO_4 tetrahedron on the 5%Na_2WO_4/SiO_2 catalyst was distorted by the interaction of crystalline Na_2WO_4 with the SiO_2 support.[10] This is contrary to the results presented here since crystalline Na_2WO_4 does not interact with the SiO_2 support and the surface sites are responsible for the appearance of the Raman band originating from the dispersed phase Na–WO_4 surface sites. Lastly, it can be noted that a handful of previous reports hypothesized about the pseudo-tetrahedral WO_4 as being the active site for OCM.[10,19,50,51] However, none of these reports confirmed the presence of dispersed phase Na–WO_4 sites or the effect of Na-coordination on the WO_4 structure. The present work shows that the presence of various catalyst phases (crystalline *vs.* dispersed *vs.* nanoparticles) is possible. Furthermore, the association of the activity during OCM with the WO_4 units in the crystalline Na_2WO_4 phase is inaccurate since crystalline Na_2WO_4 melts at ~700 °C and is not present under OCM conditions.

Conclusions

Application of modern *in situ* physical (Raman, IR, UV-vis) and chemical probe (TPSR, TPR) spectroscopic techniques has provided new insights into supported Na–WO_x/SiO_2 catalysts during OCM. The traditionally prepared catalysts corresponding to 5%Na_2WO_4 nominal loading with a Na/W molar ratio of 2, especially from the $Na_2WO_4{\cdot}2H_2O$ precursor, resulted in catalysts with SiO_2 in the cristobalite phase co-populated with crystalline Na_2WO_4 (Na/W = 2) and dispersed Na–WO_4 (Na/W < 2) phases. In contrast, the catalysts prepared *via* a modified impregnation method using individual precursors NaOH + AMT in carefully controlled proportions to maintain the Na/W molar ratio well below 2 resulted in catalysts with SiO_2 in the amorphous phase, populated only with dispersed phase Na–WO_4 surface sites with Na/W < 2. The dispersed phase Na–WO_4 surface sites with Na/W < 2 were found to be more geometrically distorted, less basic in nature, and more reducible than crystalline Na_2WO_4 (Na/W = 2). Moreover, $CH_4 + O_2$ TPSR results provide direct experimental evidence that the catalyst with only dispersed phase Na–WO_4 sites with Na/W < 2 was less active for the formation of CO_x products (hence, more selective) and initiated C_2H_6 formation at higher temperature (hence, less active) than the traditional Na_2WO_4/SiO_2 (Na/W = 2) catalyst that contains both dispersed and crystalline phases. For the first time, the present investigation establishes the identity and crucial role of the dispersed phase, Na-coordinated, pseudo-tetrahedral WO_4 sites on the SiO_2 support surface in methane activation during OCM. Moreover, the long speculated role of the crystalline cristobalite phase of SiO_2 towards OCM has been experimentally disproven, since the catalysts with Na/W < 2 retain SiO_2 in the amorphous phase due to the low concentrations of Na available, yet produce better final catalysts than their cristobalite supported counterparts.

Conflicts of interest

There are no conflicts of interest to declare.

Acknowledgements

This work was supported by NSF CBET award # 1706581. DK and SS performed all experimental work. DK, SS, JB, and IEW designed the experimental strategy and wrote the manuscript. The authors also gratefully acknowledge insightful input from Dr. Michael E. Ford of the *Operando* Molecular Spectroscopy & Catalysis Research Laboratory at Lehigh University. Q11

References

1 B. Wang, S. Albarracín-Suazo, Y. Pagán-Torres and E. Nikolla, Advances in Methane Conversion Processes, *Catal. Today*, 2017, **285**, 147–158.
2 G. E. Keller and M. M. Bhasin, Synthesis of Ethylene via Oxidative Coupling of Methane: I. Determination of Active Catalysts, *J. Catal.*, 1982, **73**(1), 9–19.
3 T. N. Nguyen, T. T. P. Nhat, K. Takimoto, A. Thakur, S. Nishimura, J. Ohyama, I. Miyazato, L. Takahashi, J. Fujima and K. Takahashi, *et al.* High-Throughput Experimentation and Catalyst Informatics for Oxidative Coupling of Methane, *ACS Catal.*, 2020, **10**(2), 921–932.
4 U. Zavyalova, M. Holena, R. Schlögl and M. Baerns, Statistical Analysis of Past Catalytic Data on Oxidative Methane Coupling for New Insights into the Composition of High-Performance Catalysts, *ChemCatChem*, 2011, **3**(12), 1935–1947.
5 B. L. Farrell, V. O. Igenegbai and S. Linic, A Viewpoint on Direct Methane Conversion to Ethane and Ethylene Using Oxidative Coupling on Solid Catalysts, *ACS Catal.*, 2016, **6**(7), 4340–4346.
6 P. Schwach, X. Pan and X. Bao, Direct Conversion of Methane to Value-Added Chemicals over Heterogeneous Catalysts: Challenges and Prospects, *Chem. Rev.*, 2017, **117**(13), 8497–8520.

7 S. Arndt, T. Otremba, U. Simon, M. Yildiz, H. Schubert and R. Schomäcker, Mn–Na2WO4/SiO2 as Catalyst for the Oxidative Coupling of Methane. What Is Really Known?, *Appl. Catal., A*, 2012, **425–426**, 53–61.

8 D. Kiani, S. Sourav, J. Baltrusaitis and I. E. Wachs, The Oxidative Coupling of Methane (OCM) by SiO2-Supported Tungsten Oxide Catalysts Promoted with Mn and Na, *ACS Catal.*, 2019, **9**(7), 5912–5928.

9 S. Ji, T. Xiao, S. S.-B. Ben Li, C. Xu, R. Hou, K. S. Coleman, M. L. Green, J. Wu, S. S.-B. Ben Li and Z. C. Jiang, *et al.* Oxidative Coupling of Methane over Oxide-Supported Sodium-Manganese Catalysts, *Appl. Catal., A*, 1995, **68**(1), 191–196.

10 J. Wu and S. Li, The Role of Distorted WO4 in the Oxidative Coupling of Methane on Supported Tungsten Oxide Catalysts, *J. Phys. Chem.*, 1995, **99**(13), 4566–4568.

11 J. Wu, S. Li, J. Niu and X. Fang, Mechanistic Study of Oxidative Coupling of Methane over Mn2O3·Na2WO4SiO2 Catalyst, *Appl. Catal., A*, 1995, **124**(1), 9–18.

12 X. Fang, S. Li, J. Lin and Y. Chu, Oxidative Coupling of Methane on W-Mn Catalysts, *J. Mol. Catal.*, 1992, **6**(6), 427–433.

13 S.-B. Li, Oxidative Coupling of Methane over W-Mn/SiO2 Catalyst, *Chin. J. Chem.*, 2001, **19**(1), 16–21.

14 S. Li, Reaction Chemistry of W-Mn/SiO~ 2 Catalyst for the Oxidative Coupling of Methane, *J. Nat. Gas Chem.*, 2003, **12**(1), 1–9.

15 A. Vamvakeros, S. D. M. Jacques, V. Middelkoop, M. Di Michiel, C. K. Egan, I. Z. Ismagilov, G. B. M. Vaughan, F. Gallucci, M. van Sint Annaland and P. R. Shearing, *et al.* Real Time Chemical Imaging of a Working Catalytic Membrane Reactor during Oxidative Coupling of Methane, *Chem. Commun.*, 2015, **51**(64), 12752–12755.

Q12 16 D. Matras, A. Vamvakeros, S. Jacques, N. Grosjean, B. Rollins, S. Poulston, G. B. G. Stenning, H. Godini, J. Drnec and R. J. Cernik, *et al.* Effect of Thermal Treatment on the Stability of Na-Mn-W/SiO2 Catalyst for the Oxidative Coupling of Methane, *Faraday Discuss.*, 2020.

17 N. Soultanidis, W. Zhou, A. C. Psarras, A. J. Gonzalez, E. F. Iliopoulou, C. J. Kiely, I. E. Wachs and M. S. Wong, Relating N-pentane Isomerization Activity to the Tungsten Surface Density of WOx/ZrO2, *J. Am. Chem. Soc.*, 2010, **132**(38), 13462–13471.

18 S. Ji, T. Xiao, S. Li, C. Xu, R. Hou, K. S. Coleman and M. L. H. Green, The Relationship between the Structure and the Performance of Na-W-Mn/SiO2 Catalysts for the Oxidative Coupling of Methane, *Appl. Catal., A*, 2002, **225**(1–2), 271–284.

19 S. Ji, T. Xiao, S. Li, L. Chou, B. Zhang, C. Xu, R. Hou, A. P. E. E. York and M. L. H. H. Green, Surface WO4 Tetrahedron: The Essence of the Oxidative Coupling of Methane over M-W-Mn/SiO2catalysts, *J. Catal.*, 2003, **220**(1), 47–56.

20 I. E. Wachs, J.-M. Jehng and W. Ueda, Determination of the Chemical Nature of Active Surface Sites Present on Bulk Mixed Metal Oxide Catalysts, *J. Phys. Chem. B*, 2005, **109**(6), 2275–2284.

21 S. P. Phivilay, C. A. Roberts, A. A. Puretzky, K. Domen and I. E. Wachs, Fundamental Bulk/Surface Structure – Photoactivity Relationships of Supported {Rh(2–y)Cr(y)O3}/GaN Photocatalysts, *J. Phys. Chem. Lett.*, 2013, **4**, 3719–3724.

22 S. P. Phivilay, A. A. Puretzky, K. Domen and I. E. Wachs, Nature of Catalytic Active Sites Present on the Surface of Advanced Bulk Tantalum Mixed Oxide Photocatalysts, *ACS Catal.*, 2013, **3**, 2920–2929.

23 M. Zhu, P. Tian, R. Kurtz, T. Lunkenbein, J. Xu, R. Schlögl, I. E. Wachs and Y.-F. Han, Strong Metal–Support Interactions between Copper and Iron Oxide during the High-Temperature Water-Gas Shift Reaction, *Angew. Chem., Int. Ed.*, 2019, **58**(27), 9083–9087.

24 D. S. Kim, M. Ostromecki and I. E. Wachs, Surface Structures of Supported Tungsten Oxide Catalysts under Dehydrated Conditions, *J. Mol. Catal. A: Chem.*, 1996, **106**(1–2), 93–102.

25 E. L. Lee and I. E. Wachs, In Situ Spectroscopic Investigation of the Molecular and Electronic Structures of SiO2 Supported Surface Metal Oxides, *J. Phys. Chem. C*, 2007, **111**(39), 14410–14425.

26 E. I. Ross-medgaarden and I. E. Wachs, Structural Determination of Bulk and Surface Tungsten Oxides with UV-Vis Diffuse Reflectance Spectroscopy and Raman Spectroscopy, *J. Phys. Chem. C*, 2007, **111**(41), 15089–15099.

27 S. Lwin, Y. Li, A. I. Frenkel and I. E. Wachs, Nature of WOx Sites on SiO2 and Their Molecular Structure–Reactivity/Selectivity Relationships for Propylene Metathesis, *ACS Catal.*, 2016, **6**(5), 3061–3071.

28 M. M. Ostromecki, L. J. Burcham, I. E. Wachs, N. Ramani and J. G. Ekerdt, The Influence of Metal Oxide Additives on the Molecular Structures of Surface Tungsten Oxide Species on Alumina. II. In Situ Conditions, *J. Mol. Catal. A: Chem.*, 1998, **132**(1), 59–71.

29 J. Wu and S. Li, The Role of Distorted W04 in the Oxidative Coupling of Methane on Tungsten Oxide Supported Catalysts, *J. Phys. Chem.*, 1995, **99**, 4566–4568.

30 J. T. Grant, C. A. Carrero, A. M. Love, R. Verel and I. Hermans, Enhanced Two-Dimensional Dispersion of Group v Metal Oxides on Silica, *ACS Catal.*, 2015, **5**(10), 5787–5793.

31 H. Tian, C. A. Roberts and I. E. Wachs, Molecular Structural Determination of Molybdena in Different Environments: Aqueous Solutions, Bulk Mixed Oxides, and Supported MoO3 Catalysts, *J. Phys. Chem. C*, 2010, **114**(33), 14110–14120.

32 E. I. Ross-Medgaarden, W. V. Knowles, T. Kim, M. S. Wong, W. Zhou, C. J. Kiely and I. E. Wachs, New Insights into the Nature of the Acidic Catalytic Active Sites Present in ZrO2-Supported Tungsten Oxide Catalysts, *J. Catal.*, 2008, **256**(1), 108–125.

33 S. S. Chan, I. E. Wachs, L. L. Murrell, L. Wang and W. K. Hall, In Situ Laser Raman Spectroscopy of Supported Metal Oxides, *J. Phys. Chem.*, 1984, **88**(24), 5831–5835.

34 S. S. Chan and I. E. Wachs, In Situ Laser Raman Spectroscopy of Nickel Oxide Supported on γ-Al2O3, *J. Catal.*, 1987, **103**(1), 224–227.

35 M. Zhu, B. Li, J.-M. M. Jehng, L. Sharma, J. Taborda, L. Zhang, E. Stach, I. E. Wachs, Z. Wu and J. Baltrusaitis, Molecular Structure and Sour Gas Surface Chemistry of Supported K2O/WO3/Al2O3catalysts, *Appl. Catal., B*, 2018, **232**, 146–154.

36 D. Kiani, G. Belletti, P. Quaino, F. Tielens and J. Baltrusaitis, Structure and Vibrational Properties of Potassium-Promoted Tungsten Oxide Catalyst Monomeric Sites Supported on Alumina (K2O/WO3/Al2O3) Characterized Using Periodic Density Functional Theory, *J. Phys. Chem. C*, 2018, **122**, 24190–24201.

37 W. E. Taifan, Y. Li, J. P. Baltrus, L. Zhang, A. I. Frenkel and J. Baltrusaitis, Operando Structure Determination of Cu and Zn on Supported MgO / SiO 2 Catalysts during Ethanol Conversion to 1 , 3-Butadiene, *ACS Catal.*, 2018, **9**, 269–285.

38 A. M. Turek, I. E. Wachs and E. DeCanio, Acidic Properties of Alumina-Supported Metal Oxide Catalysts: An Infrared Spectroscopy Study, *J. Phys. Chem.*, 1992, **96**(12), 5000–5007.

39 C. J. Keturakis, F. Ni, M. Spicer, M. G. Beaver, H. S. Caram and I. E. Wachs, Monitoring Solid Oxide CO2 Capture Sorbents in Action, *ChemSusChem*, 2014, **7**(12), 3459–3466.

40 G. Busca and V. Lorenzelli, Infrared Spectroscopic Identification of Species Arising from Reactive Adsorption of Carbon Oxides on Metal Oxide Surfaces, *Mater. Chem.*, 1982, **7**(1), 89–126.

41 S. M. K. Shahri and S. M. Alavi, Kinetic Studies of the Oxidative Coupling of Methane over the Mn/Na2WO4/SiO2 Catalyst, *J. Nat. Gas Chem.*, 2009, **18**(1), 25–34.

42 S. Mahmoodi, M. R. Ehsani and M. Hamidzadeh, Effect of Additives on Mn/SiO2 Based Catalysts on Oxidative Coupling of Methane, *Iran. J. Chem. Chem. Eng.*, 2011, **30**(1), 29–36.

43 I. Z. Ismagilov, E. V. Matus, V. V. Kuznetsov, M. A. Kerzhentsev, S. A. Yashnik, T. V. Larina, I. P. Prosvirin, R. M. Navarro, J. L. G. Fierro and G. Gerritsen, *et al.* Effect of Preparation Mode on the Properties of Mn-Na-W/Sio2catalysts for Oxidative Coupling of Methane: Conventional Methods vs. POSS Nanotechnology, *Eurasian Chem.-Technol. J.*, 2016, **18**(2), 93–110.

44 V. Fleischer, R. Steuer, S. Parishan and R. Schomäcker, Investigation of the Surface Reaction Network of the Oxidative Coupling of Methane over Na2WO4/Mn/SiO2 Catalyst by Temperature Programmed and Dynamic Experiments, *J. Catal.*, 2016, **341**, 91–103.

45 A. Palermo, J. P. Holgado Vazquez, A. F. Lee, M. S. Tikhov and R. M. Lambert, Critical Influence of the Amorphous Silica-to-Cristobalite Phase Transition on the Performance of Mn/Na2WO4/SiO2 Catalysts for the Oxidative Coupling of Methane, *J. Catal.*, 1998, **177**(2), 259–266.

46 A. Malekzadeh, M. Abedini, A. A. Khodadadi, M. Amini, H. K. Mishra and A. K. Dalai, Critical Influence of Mn on Low-Temperature Catalytic Activity of Mn/Na2WO4/SiO2 Catalyst for Oxidative Coupling of Methane, *Catal. Lett.*, 2002, **84**(1), 45–51.

47 L. Tang, J. Choi, W. J. Lee, J. Patel and K. Chiang, Metal Effects in Mn-Na2WO4/SiO2 upon the Conversion of Methane to Higher Hydrocarbons, *Adv. Energy Res.*, 2017, **5**(1), 13–29. Q13

48 N. S. Hayek, N. S. Lucas, C. Warwar Damouny and O. M. Gazit, Critical Surface Parameters for the Oxidative Coupling of Methane over the Mn–Na–W/SiO $_2$ Catalyst, *ACS Appl. Mater. Interfaces*, 2017, **9**(46), 40404–40411.

49 Z. C. Jiang, C. J. Yu, X. P. Fang, S. B. Li and H. L. Wang, Oxide/Support Interaction and Surface Reconstruction in the Sodium Tungstate(Na2WO4)/Silica System, *J. Phys. Chem.*, 1993, **97**(49), 12870–12875. Q14

50 Y. Kou, B. Zhang, J. Niu, S. Li, H. Wang, T. Tanaka and S. Yoshida, Amorphous Features of Working Catalysts: XAFS and XPS Characterization of Mn/Na2WO4/SiO2as Used for the Oxidative Coupling of Methane, *J. Catal.*, 1998, **173**(2), 399–408.

51 W. Pengwei, Z. Guofeng, Y. Wang, L. Yong, P. Wang, G. Zhao, Y. Wang and Y. Lu, MnTiO3-Driven Low-Temperature Oxidative Coupling of Methane over TiO2-Doped Mn2O3-Na2WO4/SiO2catalyst, *Sci. Adv.*, 2017, **3**(6), 1–10.